Environmental Science and Pollution Research (2021) 28:31630–31639
https://doi.org/10.1007/s11356-021-12797-x

RESEARCH ARTICLE

# Template synthesis of ordered mesoporous MgO with superior adsorption for Pb(II) and Cd(II)

Zhiping Liu[1] · Cong Li[1] · Mengjie Kuang[1] · Baixiong Liu[1] · Bin Yang[1]

Received: 26 October 2020 / Accepted: 1 February 2021 / Published online: 20 February 2021


## Abstract

Ordered mesoporous MgO was synthesized via template method by using magnesium nitrate as a precursor and amphiphilic triblock copolymer Pluronic F127 as a template. The products were characterized by X-ray powder diffraction (XRD) and transmission electron microscopy (TEM), and the Brunauer-Emmett-Teller (BET) method was used to calculate the specific surface areas. The effects of aging time, relative humidity, and magnesium nitrate content on the morphology and textural properties of the products were studied. When the aging time was 36 h and the relative humidity was 40%, the ordered mesoporous MgO with uniform pore sizes (3.2 nm), high specific surface areas (517.2 $m^2/g$), and high pore volumes (0.42 $cm^3/g$) were obtained. Furthermore, the adsorption properties of ordered mesoporous MgO as adsorbent for removal of Pb(II) and Cd(II) ions were studied. The adsorption kinetics and isotherm data agreed well with pseudo-second-order model and Langmuir model, indicating that the adsorption of heavy metal ions on the ordered mesoporous MgO was mainly chemical and homogeneous adsorption. The maximum adsorption capacities for Pb(II) and Cd(II) ions were up to 3073.5 mg/g and 1485.1 mg/g, respectively.

**Keywords** Mesoporous · Magnesium oxide · Template method · Adsorption · Heavy metal ions

## Introduction

As we all know, freshwater is an essential resource for the survival of all life on Earth. However, with the rapid development of modern industrialization, the environmental water pollution is becoming more and more serious (Wu et al. 2017). Among various sources of water pollution, heavy metal ions have been considered as one of the most toxic pollutions because of their non-degradable and accumulative nature (Bhatnagar et al. 2011; Wang et al. 2013; Yu et al. 2018). Excessive concentrations of heavy metal ions like Pb(II) and Cd(II) in water can cause serious human health problems, such as heart disease, bladder cancer, leukemia, and thyroid disorder (Liu et al. 2014; Qu et al. 2013). Therefore, highly effective adsorption of them from water is of great importance. To the best of our knowledge, various conventional methods like ion exchange, precipitation, adsorption, and evaporation have been used for wastewater purification (Iannazzo et al. 2017; Kumar et al. 2013; Li and Zhou 2018; Mahmood et al. 2011). Among them, the adsorption method has been widely used because of its simplicity and high efficiency for heavy metal ion removal (Sheela et al. 2011; Xiong et al. 2015; Yu et al. 2011). Till now, a few of traditional adsorbents such as $WO_3$, $TiO_2$, CuO, and activated alumina have been extensively utilized for the adsorptive removal of heavy metal ions from wastewater (Karami 2013; Liu et al. 2009; Özdemir et al. 2006; Zhao et al. 2011). However, these adsorbents suffer from the problem of low adsorption capacity, which greatly limit their application. Thus, it is very necessary and meaningful to synthesize new adsorbent materials with low cost and high adsorption performance.

In recent years, ordered mesoporous materials have attracted extensive attention owing to their unique structure. These materials have been widely applied in many applications such as separation, adsorption, photonic crystals, and supercapacitor electrodes (Abdusalam et al. 2017; Fan et al.

Responsible Editor: Tito Roberto Cadaval Jr

✉ Baixiong Liu
liubaixiong@jxust.edu.cn

✉ Bin Yang
yangbin@jxust.edu.cn

[1] Faculy of Materials Metallurgy and Chemistry, Jiangxi University of Science and Technology, Ganzhou, Jiangxi, China

2007; Han et al. 2012; She et al. 2011). Among them, mesoporous metal oxides with high specific surface area and uniform pore size distribution exhibit excellent adsorption efficiency for the removal of heavy metal ions from wastewater, which are considered good adsorbents (Sharma et al. 2019). Magnesium oxide (MgO), a non-toxic and environment friendly functional metal oxide, has been widely studied as an adsorbent for water purification. To date, lots of methods have been developed to synthesize mesoporous MgO nanostructures, including hydrothermal (Liu et al. 2015), sol-gel (Niesz et al. 2005), chemical gas phase deposition (Lazaridis et al. 2007), surfactant method (Possato et al. 2020), and spray-drying method (Kuang et al. 2019). Chowdhury et al. (2016) synthesized mesoporous nanostructured MgO by hydrothermal method, which exhibited excellent adsorption capacity for the removal of heavy metal ions. Yu et al. (2018) reported that MgO mesoporous nanofibers had the superior adsorption capacity of 237.49 mg/g for fluoride and 4802.27 mg/g for Congo red. Feng et al. (2015) synthesized hexagonal mesoporous MgO nanosheets with the maximum Ni(II) adsorption capacity of 1684.25 mg/g. Kuang et al. (2019) had synthesized hollow mesoporous MgO spheres by spray-drying method with improved adsorption capacity for Pb(II) and Cd(II) ions. Although various MgO nanomaterials have been successfully synthesized by different technologies, challenges still remain in the development of nanostructured MgO with high specific surface area and superior adsorption performance for Pb(II) and Cd(II) removal.

In this paper, ordered mesoporous MgO nanostructures were synthesized based on the template method by using magnesium nitrate as a precursor and amphiphilic triblock copolymer Pluronic F127 as a template. The effect of aging time, relative humidity, and magnesium nitrate content on the morphology and textural properties of the products was investigated. Furthermore, we studied the adsorption capacity of the resultant mesoporous MgO nanostructures on Pb(II) and Cd(II) ions. The adsorption isotherms and adsorption kinetics were also studied to reveal the adsorption mechanism. The as-synthesized mesoporous MgO nanostructures could be developed as potential adsorbents for highly effective adsorption of heavy metal ions in wastewater treatment.

## Experiments

### Materials

Triblock copolymer Pluronic F127 was purchased from Sigma Company. Magnesium nitrate hexahydrate ($Mg(NO_3)_2{\cdot}6H_2O$), phenol, formalin solution (37 wt%), sodium hydroxide, hydrochloric acid, ethanol, lead nitrate ($Pb(NO_3)_2{\cdot}4H_2O$), and cadmium nitrate ($Cd(NO_3)_2{\cdot}4H_2O$) were purchased from Beijing Chemicals Reagent Company (Beijing, China). All the chemical reagents in our experiment were analytically graded and used directly without further purification.

### Preparation of resol precursors

First, 8.0 g phenol and 0.36 g NaOH were dissolved in 1.7 g deionized water at room temperature. Then, 14.5 g formaldehyde solution was dropped into this solution. The mixed solution was heated to 75 °C for 1.5 h. After cooling to room temperature, the pH value was adjusted to 7.0. The solution was placed in a vacuum oven at 45 °C to remove water. Finally, the resol precursors were re-dissolved in ethanol to prepare a solution with 20 wt%.

### Preparation of mesoporous MgO

In a typical preparation, 1.0 g F127 was dissolved in 20 g ethanol and stirred for 1 h at 40 °C to form a clear solution. Subsequently, 0.1–0.4 g $Mg(NO_3)_2{\cdot}6H_2O$ and 5 g resol solution were added in sequence. After stirring at room temperature for 2 h, the mixture was dried at 30 °C for 4 h and then aged for 36 h at 40% relative humidity (RH) in an oven. Then, the as-made membranes were scraped from the glass and were calcined at different temperatures under nitrogen atmosphere with a heating rate of 1 °C/min in a tube furnace. The process was first suspended at 350 °C for 3 h and at 600 °C for 2 h. After cooling to room temperature, the products were ground into fine powders. Finally, the powders were calcined at 350 °C for 1 h under oxygen atmosphere with a heating rate of 5 °C/min in tube furnace.

### Characterization

The phase of the powders was characterized by X-ray diffractometer (XRD, Rigku D-max 2500) with Cu Kα radiation ($\lambda$ = 0.15 nm) at a scanning speed 3°/min. The morphologies of the samples were characterized by using transmission electron microscopy (TEM) (Tecnai G2 30ST), with an accelerating voltage of 300 kV. The $N_2$ adsorption and desorption isotherms were measured by using Micromeritics ASAP 2020 to characterize the adsorption types, and the specific surface areas and pore size distributions were calculated by the Brunauer-Emmett-Teller (BET) and Barrett–Joyner–Halenda (BJH) methods, respectively. The inductively coupled plasma-atomic emission spectroscopy (ICP-AES, Jarrell-Ash model ICAP 9000) was utilized to determine the concentrations of heavy metal ions remaining in solutions after adsorption.

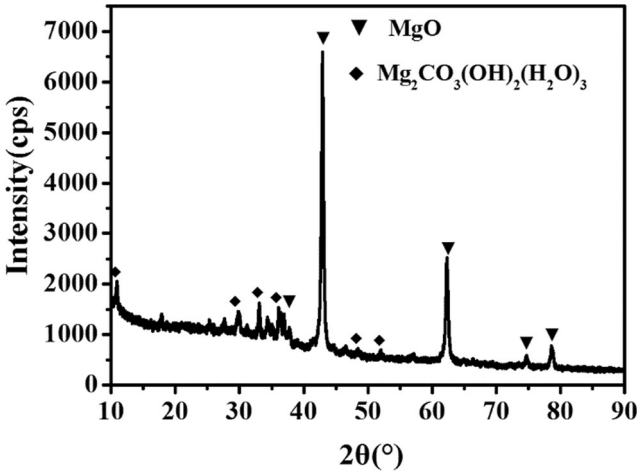


**Fig. 1** XRD pattern of prepared mesoporous MgO calcined at 350 °C

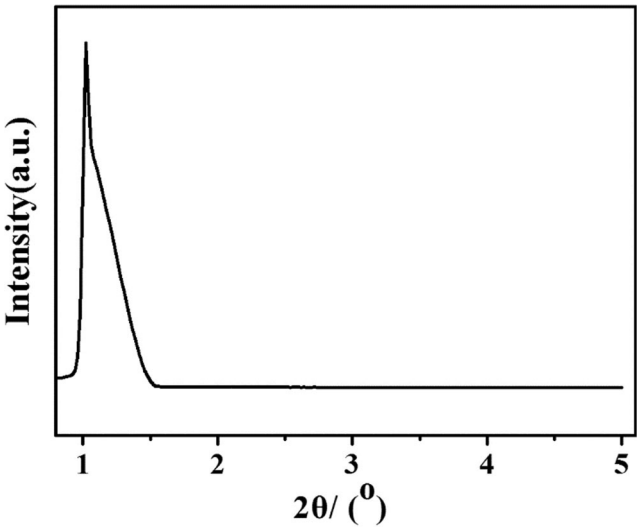


**Fig. 3** SAXRD pattern of the synthesized mesoporous MgO calcined at 600 °C

## Heavy metal ions adsorption test

Pb(II) and Cd(II) ion solutions with different concentrations were prepared by using lead nitrate and cadmium nitrate as the sources of heavy metal ions, respectively. The pH values of each Pb(II) and Cd(II) ion solution were 5.0. The mesoporous MgO powders obtained by calcination at 350 °C were used as adsorbent. For the adsorption kinetic study, 200 mg mesoporous MgO powders were added into 200 mL Pb(II) and Cd(II) solutions with an initial concentration of 100 mg/L, respectively. After stirring at specified time, the solid and liquid were separated immediately, and the concentrations of residual heavy metal ions in the supernatant after centrifugation were measured by the inductively coupled plasma-atomic emission spectroscopy (ICP). For the adsorption isothermal study, 20 mg of mesoporous MgO was added to 20 mL solutions with different concentrations of Pb(II) and Cd(II) ions under stirring at room temperature (25 °C) for 24 h.

The adsorption capacity ($q_e$, mg/g) of MgO for adsorbing heavy metal ions was calculated by the formula:

$$q_e = \frac{V(C_0 - C_e)}{m} \quad (1)$$

where $C_0$ (mg/L) is the initial concentrations of heavy metal ions and $C_e$ (mg/L) is the equilibrium concentrations, while $V$ (L) is the volume of the solution and $m$ (g) is the weight of the adsorbent.

## Results and discussion

### Structures and morphologies of the synthesized mesoporous MgO

The XRD pattern of mesoporous MgO powders calcined at 350 °C is shown in Fig. 1. It is obvious that the diffraction peaks can be indexed to MgO (JCPDS # 79-0612) and $Mg_2CO_3(OH)_2(H_2O)_3$ (JCPDS # 70-0591) phases. Among them, $Mg_2CO_3(OH)_2(H_2O)_3$ phase was formed by the combination of MgO with $CO_2$ produced during decarbonization and $H_2O$ in the environment (Yan and Xue 2005). The reaction equation is presented as follows:

$$MgO + CO_2 + H_2O \rightarrow Mg_2CO_3(OH)_2(H_2O)_3 \quad (2)$$

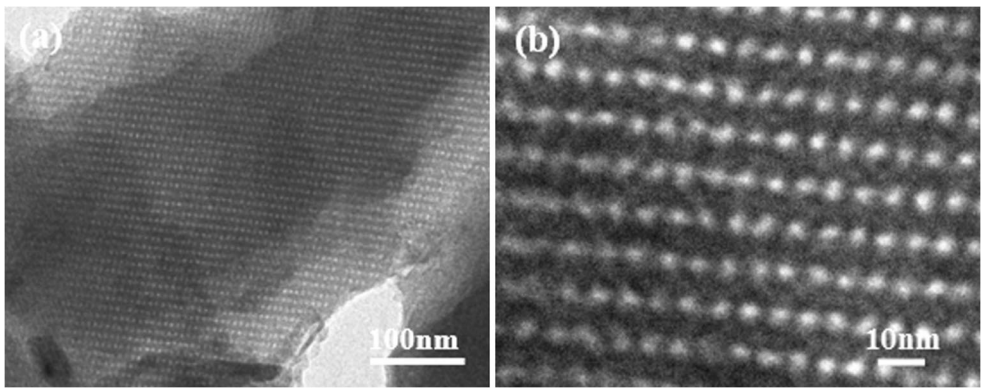


**Fig. 2** TEM image (**a**) and the amplification TEM image (**b**) of as-prepared mesoporous MgO calcined at 600 °C

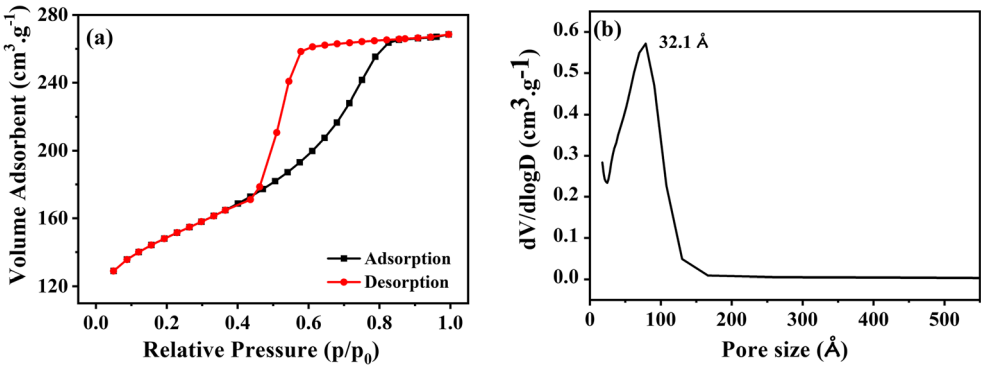


**Fig. 4** $N_2$ adsorption-desorption isotherms (**a**) and pore size distribution curve (**b**) for the synthesized samples calcined at 350 °C

In addition, the diffraction peaks of MgO were obvious and sharp, indicating that the samples had good crystallinity after calcination at 350 °C.

Figure 2 a shows the TEM image of as-prepared mesoporous MgO calcined at 600 °C. As shown in Fig. 2a, the as-prepared mesoporous MgO exhibits large domains of typical stripe-like and hexagonally arranged patterns, indicating that a highly ordered mesostructure is formed in the as-prepared mesoporous MgO (Li et al. 2021). The high-magnification TEM image (Fig. 2b) further reveals that the as-prepared mesoporous MgO exhibits 2-D hexagonal mesostructured with average pore diameter of ~ 3 nm.

The small-angle XRD (SAXRD) pattern of mesoporous MgO powders calcined at 600 °C is shown in Fig. 3. It displays an obvious small diffraction peak at $2\theta$ of 1.05°, indicating that the MgO structure still maintains an obvious mesoporous structure without collapse (Babu et al. 2012), which is consistent with the above TEM surface morphology.

The $N_2$ adsorption-desorption isotherms and pore size distributions via the BJH method of the as-prepared MgO powders calcined at 350 °C are shown in Fig. 4. The isotherm exhibits a typical Langmuir IV isotherm with H2 hysteresis loop, indicating the existence of mesostructure in the as-prepared MgO (Biabani et al. 2012; Li et al. 2021). Moreover, obvious capillary condensation was observed at a relative pressure ($P/P_0$) of 0.45–0.83, which reflects a high-uniformity mesopores (She et al. 2011). The corresponding BJH pore size distributions derived from the desorption data of the isotherms are shown in the inset of Fig. 4. It can be seen that the pore size distribution was narrow and mainly concentrated in the range of 20–100 Å, indicating that the prepared MgO has uniform mesoporous channels. The

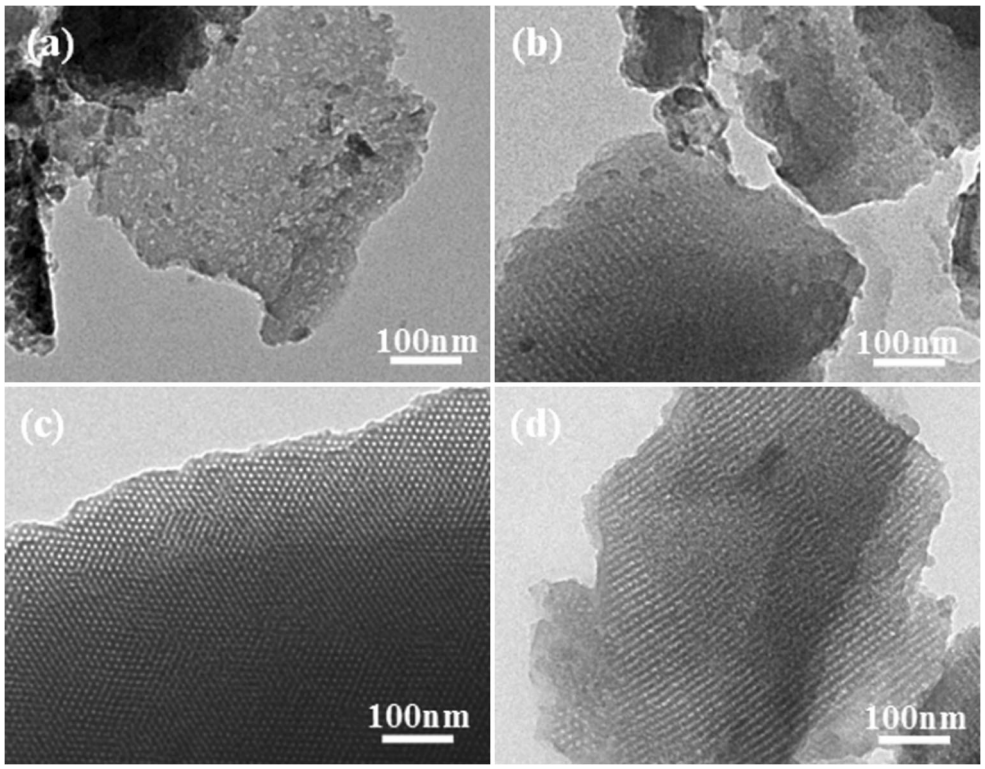


**Fig. 5** TEM images of mesoporous MgO by different aging times. **a** 12 h. **b** 24 h. **c** 36 h. **d** 48 h

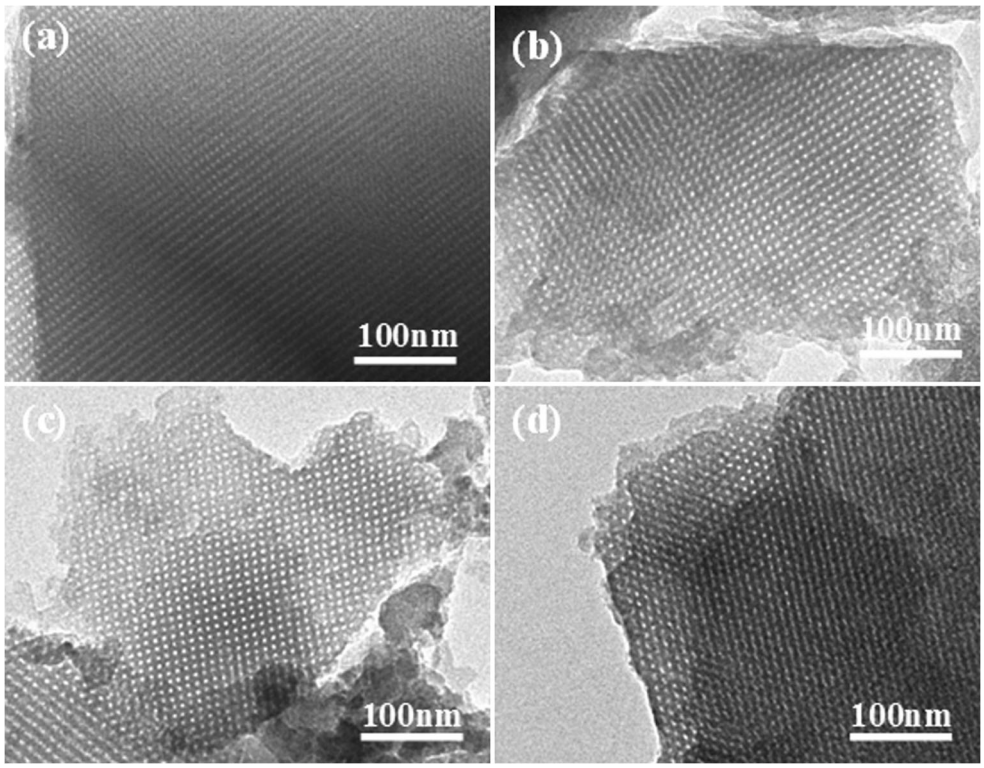


**Fig. 6** TEM images of mesoporous MgO prepared at different relative humidities (RHs). **a** 30% RH. **b** 35% RH. **c** 40% RH. **d** 45% RH

calculated pore size of the sample is 3.2 nm, the specific surface area is 517.5 $m^2/g$, and the pore volume is 0.4152 $cm^3/g$. According to the above analysis results, mesoporous MgO materials with ordered arrangement pores were successfully prepared by template method.

## Effect of aging time

The aging conditions of the membranes play an important role in the formation of mesoporous structures. We examined the effect of aging time on the morphology and textural properties of the products. The TEM images of mesoporous MgO powders by different aging time are shown in Fig. 5. It can be clearly seen that when the aging time is 12 h, the sample has few and disordered mesoporous structures (Fig. 5a). As the aging time extended to 24 h (Fig. 5b), the obtained MgO material has a large number of mesoporous structures, and is undergoing self-assembly sequence of micelle contraction and closing, and the pore structure changes obviously. The main reason is that the short aging time leads to a decrease in the crosslinking degree of the gel, and there is no sufficient hydrolysis and condensation process to form an unstable mesoporous structure. When the aging time is 36 h, the obtained mesoporous structure is shown in Fig. 5c, presenting regular mesoporous structure. Moreover, according to the above discussion, the membranes prepared under this condition can withstand baking at 600 °C. However, when the aging time increases to 48 h (Fig. 5b), the ordered degree of mesoporous structure of MgO decreases.

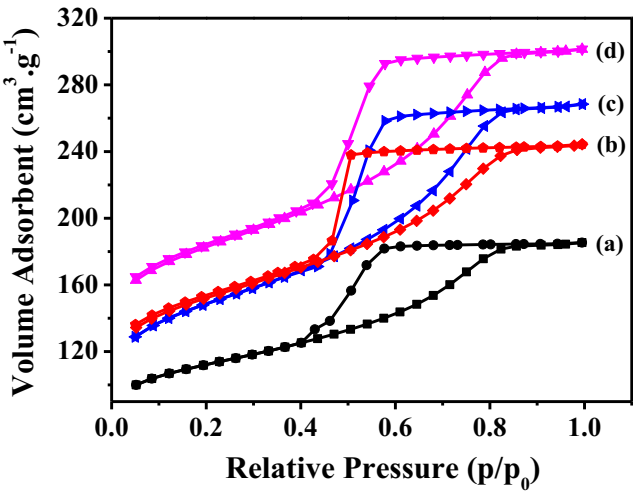


**Fig. 7** $N_2$ adsorption-desorption isotherms of the MgO synthesized by different relative humidities (RHs). **a** 30% RH. **b** 35% RH. **c** 40% RH. **d** 45% RH

**Table 1** Textural properties of different relative humidity samples

| RH (%) | 30 | 35 | 40 | 45 |
|---|---|---|---|---|
| $S_{BET}$ ($m^2/g$) | 387.7 | 530.9 | 517.5 | 526.8 |
| $D_{average}$ (nm) | 2.9 | 3.1 | 3.2 | 2.8 |
| $V$ ($cm^3/g$) | 0.29 | 0.41 | 0.42 | 0.38 |

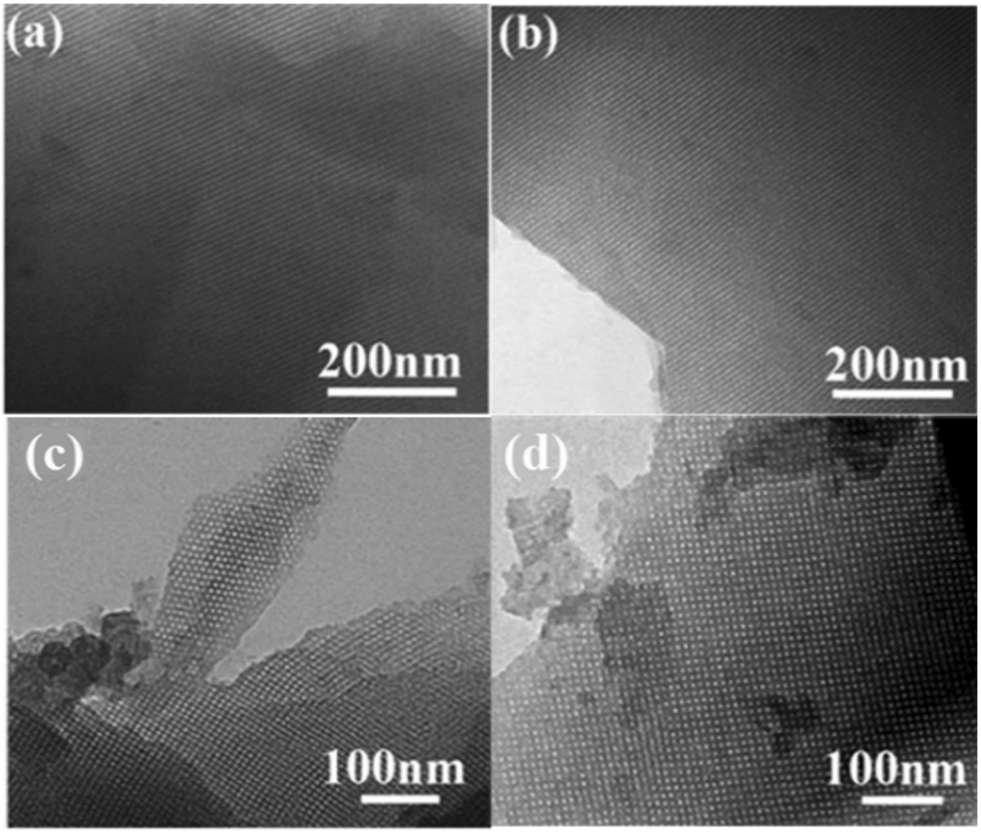


**Fig. 8** TEM images of MgO synthesized by different $Mg(NO_3)_2{\cdot}6H_2O$ contents. **a** 0.1 g $Mg(NO_3)_2{\cdot}6H_2O$. **b** 0.2 g $Mg(NO_3)_2{\cdot}6H_2O$. **c** 0.3 g $Mg(NO_3)_2{\cdot}6H_2O$. **d** 0.4 g $Mg(NO_3)_2{\cdot}6H_2O$

## Effect of relative humidity

Relative humidity is also a very important factor in the synthesis of mesoporous materials. In order to study its influence on the sample morphology, we have prepared mesoporous MgO materials by aging for 36 h under different relative humidities. Figure 6 shows the TEM images of the synthesized mesoporous MgO powders. It is obviously observed that all samples exhibit large domains of typical stripe-like and ordered arrangement.

To further study the effect of relative humidity on the pore structures of the samples, the $N_2$ adsorption-desorption isotherms and BJH calculated method were used to analyze the pore sizes and specific surface areas of the samples. As shown in Fig. 7, all synthesized mesoporous MgO exhibits a typical

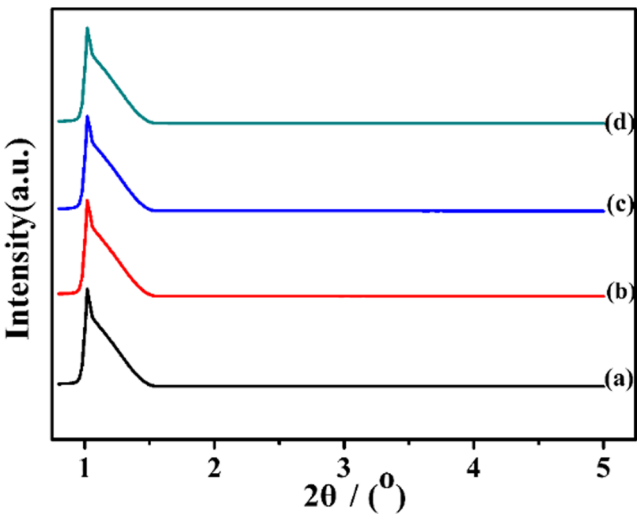


**Fig. 9** SAXRD patterns of MgO synthesized by different $Mg(NO_3)_2{\cdot}6H_2O$ contents. **a** 0.1 g $Mg(NO_3)_2{\cdot}6H_2O$. **b** 0.2 g $Mg(NO_3)_2{\cdot}6H_2O$. **c** 0.3 g $Mg(NO_3)_2{\cdot}6H_2O$. **d** 0.4 g $Mg(NO_3)_2{\cdot}6H_2O$

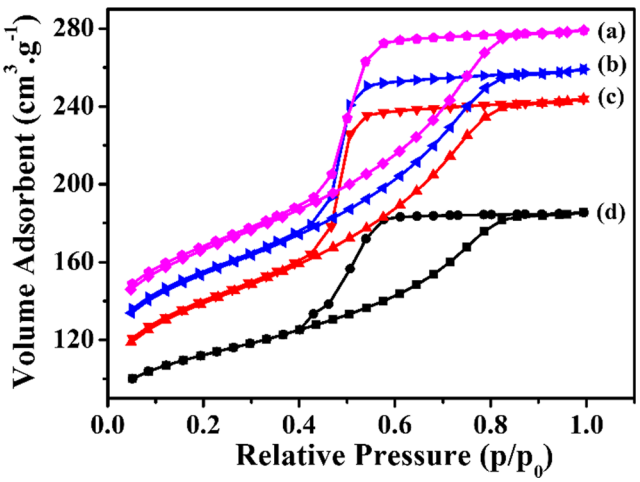


**Fig. 10** $N_2$ adsorption-desorption isotherms of MgO synthesized by different $Mg(NO_3)_2{\cdot}6H_2O$ contents. **a** 0.1 g $Mg(NO_3)_2{\cdot}6H_2O$. **b** 0.2 g $Mg(NO_3)_2{\cdot}6H_2O$. **c** 0.3 g $Mg(NO_3)_2{\cdot}6H_2O$. **d** 0.4 g $Mg(NO_3)_2{\cdot}6H_2O$

**Table 2** Physicochemical properties of MgO with different $Mg(NO_3)_2{\cdot}6H_2O$ contents

| $Mg(NO_3)_2$ $6H_2O$ (g) | 0.1 | 0.2 | 0.3 | 0.4 |
|---|---|---|---|---|
| $S_{BET}$ ($m^2/g$) | 515.9 | 454.7 | 441.4 | 382.5 |
| $D_{average}$ (nm) | 2.1 | 2.1 | 2.7 | 3.9 |
| $V$ ($cm^3/g$) | 0.27 | 0.23 | 0.29 | 0.37 |

Langmuir IV isotherm and has H2 hysteresis loop, indicating a highly uniform mesostructure (Li et al. 2021), which is consistent with the TEM result. The calculated parameters are listed in Table 1. The mean pore sizes of the mesoporous MgO prepared at different relative humidities are in the range of 2.9–3.2 nm. When the relative humidity is 30%, the specific surface areas of the sample are small and only 387.7 $m^2/g$. When the humidity is in a low range, the volatile matter in the film volatilizes at a very high speed so that the micelle does not completely shrink and close, forming particles, resulting in a low specific surface area. However, when the relative humidity is 45% RH, the pore size and volume become smaller mainly due to the high humidity and low evaporation rate, which promotes the inorganic salt oligomer to combine with EO [$HO(CH_2CH_2O)$] group of PEO (polyethylene oxide) in the inner layer of micelle, thus forming ordered mesopores with large wall thickness.

## Effect of magnesium nitrate content

In this study, the effects of magnesium nitrate content on mesoporous MgO structures were also investigated. As shown in Fig. 8, the TEM images of mesoporous MgO samples with different $Mg(NO_3)_2{\cdot}6H_2O$ contents all exhibit typical stripe-like arrangement, showing that there are 2-D hexagonal mesostructures in them. In addition, the SAXRD was also utilized to further characterize the orderliness of MgO materials synthesized by adding different $Mg(NO_3)_2{\cdot}6H_2O$ contents. As shown in Fig. 9, the samples have an obvious diffraction peak around $2\theta$ = 1.02°, indicating a hole with regular pores (Babu et al. 2012). With the increasing magnesium content, the peak intensity increased, and pores became more regular.

**Table 3** Langmuir equation parameters for Pb(II) and Cd(II) adsorption onto mesoporous MgO

| $Mg(NO_3)_2{\cdot}6H_2O$ (g) | $q_m$ (mg/g) | | $R^2$ | | ARE (%) | |
|---|---|---|---|---|---|---|
| | Pb(II) | Cd(II) | Pb(II) | Cd(II) | Pb(II) | Cd(II) |
| 0.1 | 1671.9 | 787.1 | 0.9955 | 0.9943 | 1.37 | 3.49 |
| 0.2 | 1952.6 | 992.0 | 0.9710 | 0.9764 | 4.35 | 3.14 |
| 0.3 | 2347.5 | 1325.8 | 0.9917 | 0.9916 | 2.76 | 4.39 |
| 0.4 | 3073.5 | 1485.1 | 0.9928 | 0.9951 | 5.26 | 4.01 |

As shown in Fig. 10, the $N_2$ adsorption-desorption isotherms of the mesoporous MgO materials belong to typical IV curves with H2 hysteresis loop. Obvious capillary condensation is observed at a relative pressure ($P/P_0$) of 0.45–0.8, indicating a highly uniform mesostructure (Li et al. 2021). The specific surface area, pore sizes, and pore volumes of MgO samples calculated according to BET and BJH method are shown in Table 2. The pore size of MgO is mainly distributed in the range of 2.1–3.9 nm, showing small variations with different $Mg(NO_3)_2{\cdot}6H_2O$ contents. The specific surface area gradually decreases with the increasing $Mg(NO_3)_2{\cdot}6H_2O$ contents, which is attributed to the increased ratio of high density of magnesium nitrate.

## Heavy metal ion adsorption study

To investigate the potential application of the synthesized mesoporous MgO adsorbents for heavy mental ion removal, the adsorption performance of the MgO samples for Pb(II) and Cd(II) ions was evaluated.

## Adsorption isotherm

The adsorption isotherms of different concentrations ranging from 100 to 5000 mg/L of Pb(II) and Cd(II) ions adsorbed by

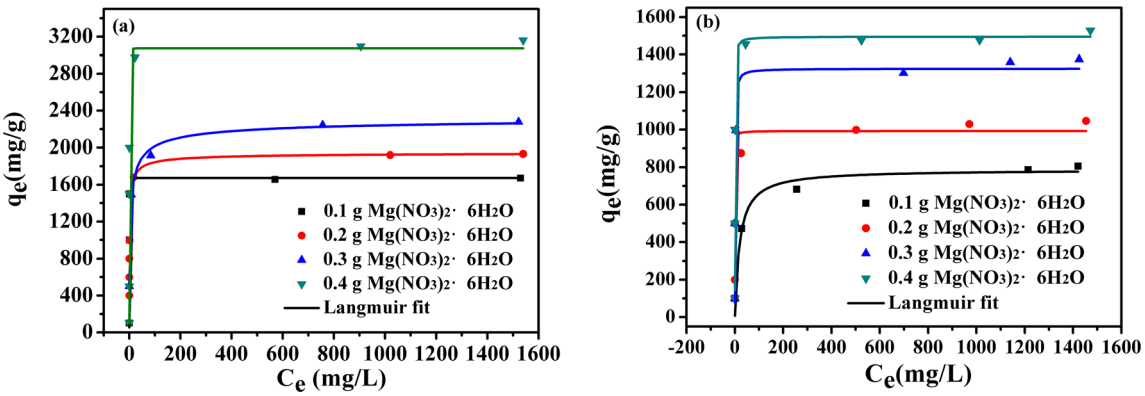


**Fig. 11** Adsorption isotherms for Pb(II) (**a**) and Cd(II) (**b**) ion adsorption onto mesoporous MgO synthesized by different $Mg(NO_3)_2{\cdot}6H_2O$ contents

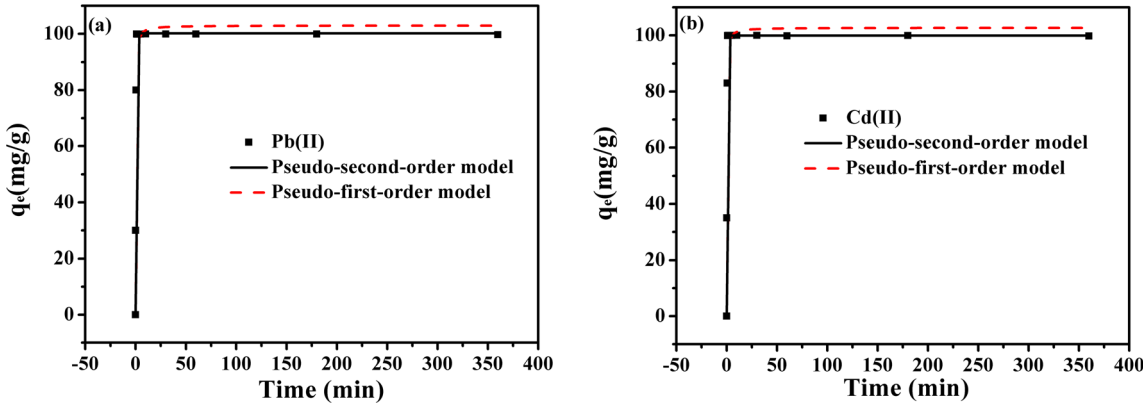


**Fig. 12** Effect of reaction time on the adsorption of Pb(II) (**a**) and Cd(II) (**b**) on ordered mesoporous MgO

MgO materials prepared with different $Mg(NO_3)_2{\cdot}6H_2O$ contents are shown in Fig. 11. The adsorption capacities were calculated using Langmuir model, expressed by the following equation:

$$q_e = \frac{q_m K_L C_e}{1 + K_L C_e} \tag{3}$$

where $q_e$ is the equilibrium adsorption capacity (mg/g), $C_e$ is the equilibrium concentration of metal ions (mg/L), $q_m$ is the maximum adsorption capacity of the adsorbent (mg/g), and $K_L$ is the adsorption constant (L/mg).

The average relative error (ARE) was applied to evaluate the fit quality according to the following equation (Alves et al. 2019):

$$\mathrm{ARE} = \frac{100}{n}\sum_i^n \left| \frac{q_{i,\mathrm{model}} - q_{i,\mathrm{exp}}}{q_{i,\mathrm{exp}}} \right| \tag{4}$$

where $q_{i,\ \mathrm{model}}$ is each value of $q$ (mg/g) predicted by the fitted model, $q_{i,\mathrm{exp}}$ is each value of $q$ measured experimentally, and $n$ is the number of experimental points.

The calculated adsorption capacities are listed in Table 3; Fig. 11 and Table 3 show that the experimental data all agree well with the Langmuir adsorption isotherm ($R^2 > 0.97$). With the increase of $Mg(NO_3)_2{\cdot}6H_2O$ contents, the saturated adsorption capacity of ordered mesoporous MgO on Pb(II) and Cd(II) ions increases gradually. When the $Mg(NO_3)_2{\cdot}6H_2O$ content increases to 0.4 g, the maximum adsorption capacities of the MgO powders for Pb(II) and Cd(II) are 3073.5 and 1485.1 mg/g, respectively. The results indicate that the synthesized mesoporous MgO is an ideal adsorbent, which can effectively remove heavy metal ions from water.

## Adsorption kinetics

The adsorption rate of Pb(II) and Cd(II) ions on mesoporous MgO adsorbents prepared by adding 0.4 g $Mg(NO_3)_2{\cdot}6H_2O$ was studied. The initial concentrations of Pb(II) and Cd(II) ions solutions were 100 mg/L. As shown in Fig. 12, the synthesized ordered mesoporous MgO adsorbent has good adsorption efficiency for Pb(II) and Cd(II) ions. After adsorption for 5 min, the adsorption capacities both reach to 99.9 mg/g, which are close to the equilibrium adsorption capacities. In the following 6 h, the adsorption capacity almost does not change, indicating that the adsorption equilibrium is established after 5 min. The results show that the prepared ordered mesoporous MgO can rapidly remove Pb(II) and Cd(II) from water.

The adsorption kinetics of Pb(II) and Cd(II) ion removal were further investigated by the pseudo-first-order and pseudo-second-order models. The pseudo-first-order and pseudo-second-order model equations are presented as follows:

$$q_t = q_e\left(1 - e^{-k_1 t}\right) \tag{5}$$

$$q_t = \frac{q_e^2 k_2 t}{1 + q_e k_2 t} \tag{6}$$

where $q_e$ and $q_t$ (mg/g) are the amounts of heavy metal ions adsorbed onto adsorbent at equilibrium and any time $t$ (min),

**Table 4** The kinetics parameters of Pb(II) and Cd(II) onto ordered mesoporous MgO

| | Pseudo-first-order | | | | Pseudo-second-order | | | |
|---|---|---|---|---|---|---|---|---|
| | $k_1$ ($\mathrm{min}^{-1}$) | $q_{e,\ \mathrm{cal}}$ (mg/g) | $R^2$ | ARE (%) | $k_2$ (g $\mathrm{mg}^{-1}$ $\mathrm{min}^{-1}$) | $q_{e,\ \mathrm{exp}}$ (mg/g) | $R^2$ | ARE (%) |
| Pb(II) | 0.0056 | 13.65 | 0.9744 | 6.23 | 0.169 | 99.93 | 0.9986 | 1.31 |
| Cd(II) | 0.0050 | 8.27 | 0.9797 | 5.09 | 0.261 | 99.97 | 0.9982 | 1.07 |

respectively. $k_1$ ($min^{-1}$) is the first-order rate constant, and $k_2$ (g $mg^{-1}$ $min^{-1}$) is the second-order rate constant.

The pseudo-first-order and pseudo-second-order kinetics model parameters are listed in Table 4. It is obvious that the linear plots are better fitted into the pseudo-second-order model with high regression coefficients ($R^2 > 0.99$), indicating that the adsorption of Pb(II) and Cd(II) on mesoporous MgO is a chemisorption process (He et al. 2019; He et al. 2020).

## Conclusion

In summary, ordered mesoporous MgO powders were successfully synthesized via template method by using magnesium nitrate as a precursor and amphiphilic triblock copolymer Pluronic F127 as a template. The effects of aging time, relative humidity, and magnesium nitrate content on the morphology and textural properties of ordered mesoporous MgO were investigated in this study. When the aging time was 36 h and the relative humidity was 40%, the synthesized mesoporous MgO exhibits uniform pore sizes (3.2 nm), high specific surface areas (517.2 $m^2$/g), and high pore volumes (0.42 $cm^3$/g). The mesoporous MgO powders prepared by adding 0.4 g magnesium nitrate showed maximum adsorption capacities up to 3073.5 and 1485.1 mg/g for Pb(II) and Cd(II) ions, respectively. The adsorption data of kinetics and isotherm fitted well with pseudo-second-order model and Langmuir isotherm model, respectively, indicating that the adsorption of Pb(II) and Cd(II) on ordered mesoporous MgO is a homogeneous and chemical adsorption process. The superior adsorption performance showed that the mesoporous MgO materials would be a promising adsorbent for Pb(II) and Cd(II) removal from water.

**Author contribution** Conceptualization, data curation, and writing—original draft: Zhiping Liu; formal analysis and validation: Cong Li; investigation: Mengjie Kuang; funding acquisition, resources, and writing—review and editing: Baixiong Liu; supervision: Bin Yang.

**Funding** This work was supported by National Natural Science Foundation of China (51664023, 51962006), Natural Science Foundation of Jiangxi Province (20202BABL204033), and Program for Excellent Young Talents, JXUST (2019006).

**Data availability** All data generated or analyzed during this study are included in this published article.

## Declarations

**Ethics approval and consent to participate** Not applicable

**Consent for publication** Not applicable

**Competing interests** The authors declare that they have no competing interests.

## References

Abdusalam D, Nataša ZT, Zorica V, Aleksandar DM, Željko R, Zlate V, Radmila JH (2017) Highly ordered macroporous γ-alumina prepared by a modified sol-gel method with a PMMA microsphere template for enhanced $Pb^{2+}$, $Ni^{2+}$ and $Cd^{2+}$ removal. Ceram Int 43:13817–13827

Alves DCS, Gonçalves JO, Coseglio BB, Burgo TAL, Dotto GL, Pinto LAA, Cadaval TRS (2019) Adsorption of phenol onto chitosan hydrogel scaffold modified with carbon nanotubes. J Environ Chem Eng 7:103460

Babu SK, Reddy AR, Sujatha C, Reddy KV (2012) Effect of Mg doping on photoluminescence of ZnO/MCM-41 nanocomposite. Ceram Int 38:5949–5956

Bhatnagar A, Kumar E, Sillanpää M (2011) Fluoride removal from water by adsorption-a review. Chem Eng J 171:811–840

Biabani A, Rezaei M, Fattah Z (2012) Optimization of preparation conditions of Fe-Co nanoparticles in low-temperature CO oxidation reaction by taguchi design method. J Nat Gas Chem 21:415–420

Chowdhury IH, Chowdhury AH, Bose P, Mandal S, Naskar MK (2016) Effect of anion type on the synthesis of mesoporous nanostructured MgO, and its excellent adsorption capacity for the removal of toxic heavy metal ions from water. RSC Adv 6:6038–6047

Fan LZ, Hu YS, Maier J, Adelhelm P, Smarsly B, Antonietti M (2007) High electroactivity of polyaniline in supercapacitors by using a hierarchically porous carbon monolith as a support. Adv Funct Mater 17:3083–3087

Feng J, Zou LY, Wang YT, Li BW, He XF, Fan ZJ, Ren YM, Lv YZ, Zhang ML, Chen D (2015) Synthesis of high surface area, mesoporous MgO nanosheets with excellent adsorption capacity for Ni(II) via a distillation treating. J Colloid Interface Sci 438:259–267

Han DZ, Li X, Zhang L, Wang YH, Yan ZF, Liu SM (2012) Hierarchically ordered meso/macroporous gamma-alumina for enhanced hydrodesulfurization performance. Microporous Mesoporous Mater 158:1–6

He XY, Min XB, Peng TY, Ke Y, Zhao FP, Wang YY, Sillanpää M (2019) Highly efficient antimonate removal from water by pyrite/hematite bi-mineral: performance and mechanism studies. J Chem Eng Data 64:5910–5919

He XY, Min XB, Peng TY, Ke Y, Zhao FP, Wang YY, Sillanpää M (2020) Enhanced adsorption of antimonate by ball-milled microscale zero valent iron/pyrite composite: adsorption properties and mechanism insight. Environ Sci Pollut R 27:16484–16495

Iannazzo D, Pistone A, Ziccarell I, Espro C, Galvagno S (2017) Removal of heavy metal ions from wastewaters using dendrimer-functionalized multi-walled carbon nanotubes. Environ Sci Pollut Res 24:14735–14747

Karami H (2013) Heavy metal removal from water by magnetic nanorods. Chem Eng J 219:209–216

Kuang MJ, Shang YS, Yang GL, Liu BX, Yang B (2019) Facile synthesis of hollow mesoporous MgO spheres via spray-drying with improved adsorption capacity for Pb(II) and Cd(II). Environ Sci Pollut Res 26:18825–18833

Kumar KY, Muralidhara HB, Nayaka YA, Balasubramanyam J, Hanumanthappa H (2013) Hierarchically assembled mesoporous ZnO nanorods for the removal of lead and cadmium by using differential pulse anodic stripping voltammetric method. Powder Technol 239:208–216

Lazaridis NK, Kyzas GZ, Vassiliou AA, Bikiaris DN (2007) Chitosan derivatives as biosorbents for basic dyes. Langmuir 23:7634–7643

Li DJ, Zhou L (2018) Adsorption of heavy metal tolerance strains to $Pb^{2+}$ and $Cd^{2+}$ in wastewater. Environ Sci Pollut Res 25:32156–32162

Li Z, Cao YJ, Li GY, Chen L, Xu WY, Zhou MJ, He BH, Wang W, Hou ZH (2021) High rate capability of S-doped ordered mesoporous carbon materials with directional arrangement of carbon layers and large d-spacing for sodium-ion battery. Electrochim Acta 366: 137466

Liu Z, Zhou A, Wang G, Zhao X (2009) Adsorption behavior of methyl orange onto modified ultrafine coal powder. Chin J Chem Eng 17: 942–948

Liu H, Gao Y, Sun L, Li M, Li B, Sun D (2014) Assessment of relationship on excess fluoride intake from drinking water and carotid atherosclerosis development in adults in fluoride endemic areas, China. Int J Hyg Environ Health 217:413–420

Liu MD, Xu J, Cheng B, Ho WK, Yu JG (2015) Synthesis and adsorption performance of $Mg(OH)_2$ hexagonal nanosheet-graphene oxide composites. Appl Surf Sci 332:121–129

Mahmood T, Saddique MT, Naeem A, Mustafa S, Dilara B, Raza ZA (2011) Cation exchange removal of Cd from aqueous solution by NiO. J Hazard Mater 185:824–828

Niesz K, Yang PD, Somorjai GA (2005) Sol-gel synthesis of ordered mesoporous alumina. Chem Commun (Camb) 15:986–1987

Özdemir Y, Dogan M, Alkan M (2006) Adsorption of cationic dyes from aqueous solutions by sepiolite. Microporous Mesoporous Mater 96: 419–427

Possato LG, Pereira E, Goncalves RGL, Pulcinelli SH, Martins L, Santilli CV (2020) Controlling the porosity and crystallinity of MgO catalysts by addition of surfactant in the sol-gel synthesis. Catal Today 344:52–58

Qu XL, Alvarez PJJ, Li QL (2013) Applications of nanotechnology in water and wastewater treatment. Water Res 47:3931–3946

Sharma M, Singh J, Hazra S, Basu S (2019) Adsorption of heavy metal ions by mesoporous ZnO and TiO2@ZnO monoliths: adsorption and kinetics studies. Microchem J 145:105–112

She L, Li J, Wan Y, Yao XD, Tu B, Zhao DY (2011) Synthesis of ordered mesoporous MgO/carbon composites by a one-pot assembly of amphiphilic triblock copolymers. J Mater Chem 21:795–800

Sheela T, Nayaka YA, Viswanatha R, Basavanna S, Venkatesha TG (2011) Kinetics and thermodynamics studies on the adsorption of Zn(II), Cd(II) and Hg(II) from aqueous solution using zinc oxide nanoparticles. Powder Technol 217:163–170

Wang S, Wei J, Lv SS, Guo Z, Jiang F (2013) Removal of organic dyes in environmental water onto magnetic-sulfonic graphene nanocomposite. Clean-Soil Air Water 41:992–1001

Wu SP, Dai XZ, Kan JR, Shilong FD, Zhu MY (2017) Fabrication of carboxymethyl chitosan-hemicellulose resin for adsorptive removal of heavy metals from wastewater. Chin Chem Let 28:625–632

Xiong CM, Wang W, Tan FT, Luo F, Chen JG, Qiao XL (2015) Investigation on the efficiency and mechanism of Cd(II) and Pb(II) removal from aqueous solutions using MgO nanoparticles. J Hazard Mater 299:664–674

Yan CL, Xue DF (2005) Novel self-assembled MgO nanosheet and its precursors. The J Phys Chem B 109:12358–12361

Yu XY, Luo T, Jia Y, Zhang YX, Liu JH, Huang XJ (2011) Porous hierarchically micro-/nanostructured MgO: morphology control and their excellent performance in As(III) and As(V) removal. J Phys Chem 115:22242–22250

Yu ZC, Xu CH, Yuan KK, Gan XZ, Zhou HF et al (2018) Template-free synthesis of MgO mesoporous nanofibers with superior adsorption for fluoride and Congo red. Ceram Int 44:9454–9462

Zhao D, Sheng G, Hu J, Chen C, Wang X (2011) The adsorption of Pb(II) on p layered double hydroxide. Chem Eng J 171:167–174